On the Static Strength of Aluminium and Carbon Fibre aircraft lap joint repairs

Siddharth Pitta[a,*], Victor de la Mora Carles[b], Francesc Roure[c], Daniel Crespo[d] and Jose. I. Rojas[a]

[a,*] *Department of Physics – Division of Aerospace Engineering, Universitat Politècnica de Catalunya, c/ Esteve Terradas 7, 08860, Castelldefels (Spain), *email: siddharth.pitta@upc.edu*

[b] *Department of Aerospace Structures and Materials, TU Delft, Kluyverweg 1, 2629, Delft (The Netherlands)*

[c] *Department of Strength of Materials and Structural Engineering, Universitat Politècnica de Catalunya, Av. Diagonal 647, 08028, Barcelona (Spain)*

[d] *Department of Physics and Barcelona Research Center in Multiscale Science and Engineering, Universitat Politècnica de Catalunya, c/ Esteve Terradas 7, 08860, Castelldefels (Spain)*

Abstract:

The behaviour of various aircraft lap joint repair configurations is investigated experimentally and numerically under static loading. The lap joints consist of aluminium alloy (AA) 2024-T3 substrates repaired with twin single-sided AA 2024-T3 or Carbon Fibre Reinforced Epoxy (CFRE) doublers. Pure riveted, pure bonded and hybrid (riveted and bonded) joints of metal-metal and metal-composite configurations are investigated. From experimental results, joints with adhesive bond showed nearly 5 times higher average strength than pure riveted joints, while hybrid joints performed better than riveted and bonded joints because of higher stiffness. On the other hand, hybrid metal–metal joint has 70% higher average strength compared to hybrid metal–composite joint. Rivet-shear has caused failure of riveted joints, and adhesive failure is observed in pure bonded joints. Hybrid joints with metal doublers have failed initially due to adhesive failure and later rivet shear. Interestingly, net-section failure is observed in composite doublers with breakage of doublers due to the presence of holes in the doublers. Experimental results are complemented with numerical analysis using commercial finite element code ABAQUS. Load-displacement curves obtained from the numerical results are in good agreement with experiments within a marginal error of 2%. In addition to load-displacement curves, a detailed stress analysis is performed numerically on metal-metal and metal-composite joints under riveted, bonded and hybrid configurations to study stress distribution on substrate and doublers. Numerical analysis showed hybrid and bonded joints have lower stresses in substrate and doublers compared to the riveted joints. Bonded joints have smoother load transfer due to the adhesive spread over a larger area. And finally, Stress Intensity Factors (SIFs) analysis is performed numerically for un-reinforced and reinforced metal substrate with a crack length of 1, 5 and 10 mm with metal and composite doublers under riveted and bonded configuration. For crack of 10 mm, 35% reduction in SIFs is observed for reinforced substrate with bonded metal or composite doublers compared to the un-reinforced cracked substrate.

Keywords: aircraft lap joint, aluminium alloy, carbon fibre reinforced epoxy, rivet, adhesive, finite element analysis

1. Introduction

Airlines aim to operate at maximum efficiency by, for instance, reducing turn-around time between flights. During this time, aircraft are inspected for any structural damages. If any part of the aircraft is found to be damaged beyond the Federal Aviation Regulation (FAR) Part 25 standards by the Federal Aviation Administration, U.S. Department of Transportation, then it has to be repaired or replaced. Maintenance is part of operating costs which include repairs, overhauls and replacement of damaged parts. Hence, repair technologies play an important role in maintenance costs.

Aircraft structures are made from numerous small parts joined to form major assemblies, in which joining techniques play an important role. Most common methods of joining are by use of mechanical fasteners: rivets, bolts, nuts, etc. Other types of joints or repair techniques involve only adhesives or combination of fasteners and adhesives. Rivets are widely used in joining, for instance, the skin panels to stringers and spars to hold them in position. Rivets are easy to install with a short repair time, cost-effective, and with high resilience and durability compared to adhesives [1]. The strength of solid rivets is better than blind rivets if both sides of the substrate are accessible, however, this is not possible in all cases. If only single-sided access is possible, then blind rivets are used to repair cracked substrates with fastened doublers. In this study, joints are analysed with blind rivets to replicate single-side access. The strength of riveted joints depends on rivet hole diameter, material properties, squeezing force and fastening pattern [2-5]. Due to the riveting process, the holes made in the plate reduce the strength of the joint and cause high-stress concentrations [6, 7]. Early failure of riveted joints in aircraft structures may be experienced due to the induced residual stresses during manufacturing [8, 9]. Stress concentrations around the holes can be reduced by cold expansion [6, 10], clamping force [16] and interference fit [11-13], increasing the static strength and fatigue resistance of the joints.

The fatigue behaviour of single- and double-rivet self-piercing riveted joints was investigated by Iyer *et al.* [14] by means of experiments and finite element analysis (FEA). These researchers used a 3D elastic finite element model and identified the gross section of crack initiation. Multiple crack propagation in aircraft skin-doubler riveted joints was investigated by Armentani *et al.* [15]. They compared the advantages and disadvantages of a dual boundary element method and a finite element model. A 3D finite element model was developed by Oskouei *et al.* [16] to simulate the clamping force and load transfer through the joint plates. This study showed that the stress concentrations can be reduced by increasing the clamping force under static tensile loads. Bolted joint structures were investigated by Kim *et al.* [17], who proposed four types of finite element models, developed with 3D solid elements and surface-to-surface contact elements between bolt head-flange interfaces, showed better agreement with experimental results among the other models.

Understanding failure modes have always been important in designing better structures. Sathiya *et al.* [18] studied the rivet load distribution in the failure and damage tolerant design of metal-metal and metal-composite civil aircraft lap joints. This study describes various methods of modelling rivets in FEA. Further experimental studies on riveted joints were conducted by Pavan *et al.* [19] and Chen *et al.* [20]. The latter researchers studied failure modes of riveted joints under tensile loading both experimentally and numerically, showed three possible failure modes for which the numerical results were in good agreement with the test results. The failure modes of fastened bolted joints can be classified into two types: basic failure and secondary failure [21, 22]. The basic failure modes are further classified into three subtypes: net-tension, shear-out and bearing. The secondary failure modes are classified into cleavage and shear-out failure.

The role of geometric parameters in the design of fastened joints should also be considered. For instance, the further the holes from the edges, the higher is the strength of the joint. Moreover, the length and width of the plates with respect to the dimensions of the fastener holes can effectively influence the failure mode of the joint [23, 24]. The failure mode of metals and composites may also depend on loading conditions. Pisano *et al.* [25] investigated failure modes of multi-pin composite laminate joints due to fastening. For single-lap aluminium alloy (AA) 2024-T3 bolted joints, the effect of geometric variables on the stress-strain distributions and the nonlinear behaviour of the joint under tension was investigated by Keikhosravy *et al.* [26]. Nabil *et al.* [27] analysed the static and fatigue behaviour of thin riveted, bonded and hybrid composite lap joints.

Adhesive bonding of structures is also an effective way of joining aerospace and automotive parts. The strength of adhesive joints is higher than pure riveted joints; the stresses are evenly distributed along the bonded area and this makes the joint more stable with respect to stress intensity factors (SIF) and stress concentrations. Many studies have been conducted on adhesively bonded composite patches to repair cracked metallic plates [28-33]. Banea *et al.* [34] investigated the effects of surface preparation, joint configuration and adhesive properties on the response of adhesively bonded composite joints. Bending can be observed in adhesively bonded single-side composite patch repairs to metallic plates. Particularly, Clark *et al.* [35] investigated bending of bonded composite repairs on cracked AA 2024-T3 plates.

Hybrid joints (using both mechanical fasteners and adhesive) are another effective method of joining repair patches, achieving high durability [36-38]; if the adhesive fails due to the defective bond line or de-bonding, the mechanical fasteners can carry the load until the following inspection [39]. The high-stress concentrations around the fastener holes in pure riveted joints can be reduced by using an adhesive between the surfaces, which improves static strength and fatigue resistance. Hybrid joints are designed to carry shear loads since adhesive bonds are strong in shear and weak in peel [40]. Several investigations on hybrid joints have been reported in the literature [41-47]. It has been observed that failure of the adhesive between the surfaces is the predominant cause of initial failure of hybrid joints.

In this research, static failure of riveted, bonded and hybrid aircraft lap joints is investigated through experiments and numerical analysis. Substrates are made from AA 2024-T3, and the behaviour of repairs made with AA 2024-T3 doublers are compared with carbon fibre reinforced epoxy (CFRE) doublers. In addition, a finite element model is developed in ABAQUS tool and is verified against the experiment results for the riveted, bonded and hybrid joints. Most of the research in the literature focuses on pure metallic riveted and bonded joints, but very few works can be found in the literature on metal–composite riveted, bonded and hybrid joints. Hence, this research will help to improve the understanding of the advantages, behaviour and limitations of various joint configurations.

2. Materials and Methods

2.1. Materials characterization

Metal substrates and doublers for experiments are prepared from a sheet of commercial AA 2024-T3. The T3 temper consists in solution heat-treatment at 480^0C for 1 hour, followed by rapid water quenching to room temperature, cold-working and natural ageing. Tables 1 and 2 shows, respectively, the mechanical properties and composition (in wt. % and at. %) for AA 2024-T3, as provided by the supplier (Kaiser Aluminium fabricated products, Spokane, USA). Substrates are machine cut by Kaiser Aluminium into rectangular plates of dimensions 171.4

mm×25.4 mm×3.175 mm. Likewise, doubler 1 and doubler 2 are machine cut into plates of dimensions 215.9 mm×25.4 mm×1.5875 mm and 165.1 mm×25.4 mm×1.5875 mm (see Fig. 1).

Aluminium alloy	Yield stress	UTS	% Area Reduction	Brinell Hardness
AA 2024-T3	316 MPa	464 MPa	20.2%	HB 123

Table 1. Mechanical properties of aluminium alloy (AA) 2024-T3, as provided by the manufacturer (Kaiser Aluminium, USA).

Aluminium alloy	Units	Si	Fe	Cu	Mn	Mg	Zn	Ti	Cr	Al
AA 2024-T3	wt. %	0.50	0.50	4.90	0.90	1.80	0.25	0.15	0.10	90.90
AA 2024-T3	at. %	0.50	0.25	2.16	0.46	2. 70	0.11	0.09	0. 05	94.31

Table 2. The chemical composition of aluminium alloy (AA) 2024-T3, as provided by the manufacturer (Kaiser Aluminium, USA).

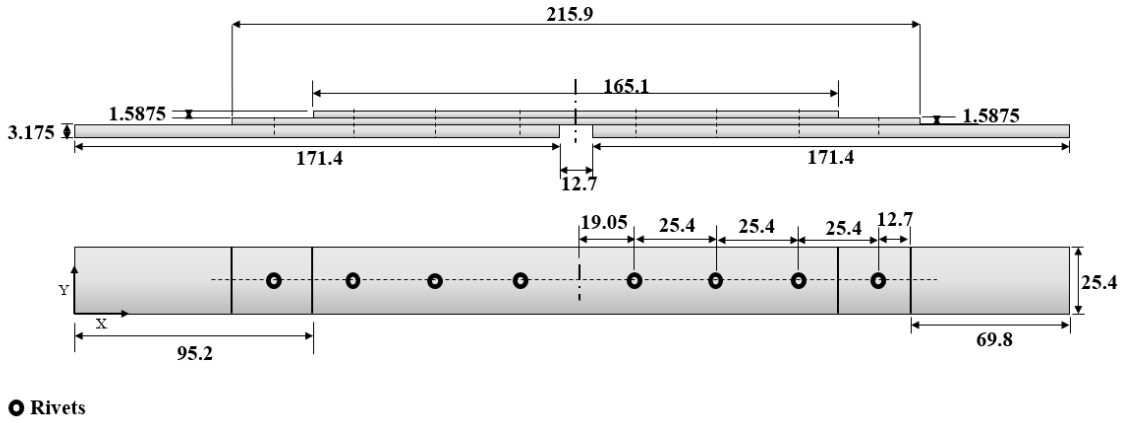

Fig. 1. Lateral view (top) and layout view (bottom) of lap joint, showing the dimensions in mm of substrate plates and twin single-sided doublers, with locations of the fastener holes.

A two-part thixotropic adhesive Araldite 2031, consisting of resin and hardener, is used in the preparation of bonded and hybrid joints. The term 'metal' corresponds to AA 2024-T3 and 'composite' corresponds to Carbon Fibre Reinforced Epoxy (CFRE). Because of bonding capability characteristic between metal-metal, metal-composite and composite-composite, Araldite 2031 is chosen for this investigation. Araldite 2031 is a toughened adhesive with high chemical resistance and has low shrinkage. The best performance can be achieved by curing the adhesive at 40^0C for 16 hours. Table 3 shows the properties of Araldite 2031, as provided by the supplier (Huntsman Advanced Materials, Switzerland GmbH). Stress-strain curve for Araldite 2031 is shown in Fig. 2. Standard aluminium pop rivets (supplied by Rapid rivets, Hestra, Sweden) are used in the preparation of riveted and hybrid joints.

Adhesive	E (GPa)	$\sigma_{fracture}$ (MPa)	$\varepsilon_{fracture}$ (%)
Araldite 2031	1.057	21.38	6.39

Table 3. Material properties of Araldite 2031, as provided by the manufacturer.

*$\sigma_{fracture}$ is the fracture stress and $\varepsilon_{fracture}$ is the fracture strain.

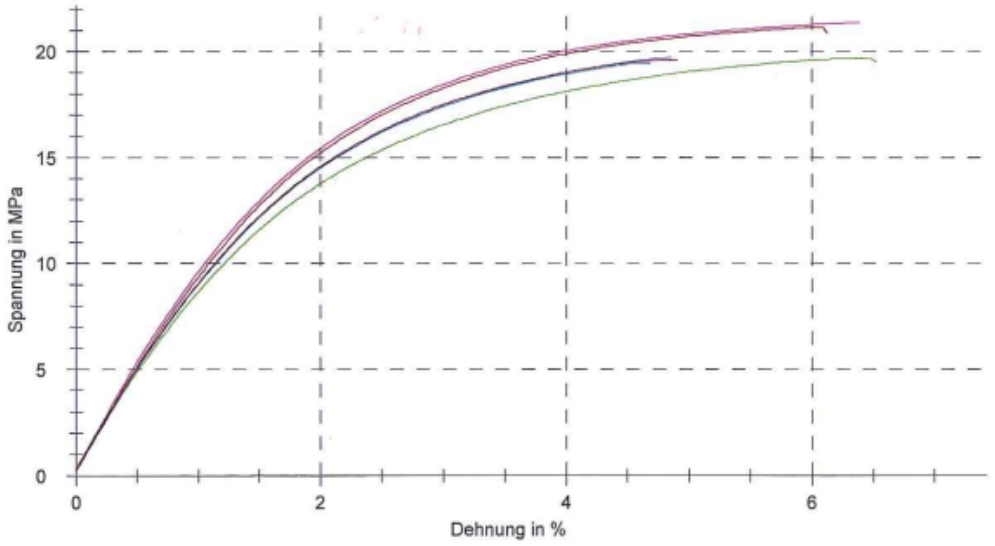

Fig. 2. Stress-strain curve for Araldite 2031 at 2 mm/min as provided by the supplier (Huntsman Advanced Materials, Switzerland).

Composite doublers are made of CFRE laminates with fibre in satin weave configuration of orientation 0^0 and 90^0 (manufactured and supplied by Composites Ate, S.L., Barcelona, Spain). Doublers are prepared by stacking six layers of plies, with ply thickness of 0.25 mm. Doublers stacking sequence is [(45/135)/ (0/90)/ (0/90)/ (0/90)/ (0/90)/ (45/135)]. Stacking sequence satisfies eight golden rules used in the aerospace industry, to make sure the composite structure has symmetry, balance, the minimum percentage of ply orientation, a maximum grouping of plies, inter-laminar shear, external plies for protecting against any damages, damage tolerance and coupling effects. By following the golden rules, doublers ensure they can carry the high load in the tensile direction (0º with the *x*-axis of the reference frame, as shown in Fig. 1). The composite material has a density of 1600 kg/m^3 with the mechanical properties shown in Table 4.

Property	E_{11} (GPa)	E_{22} (GPa)	G_{12} (GPa)	G_{13} (GPa)	ν_{12}	Tensile Strength (MPa)			Compressive Strength (MPa)	
						$+S_{11}$	$+S_{22}$	$+S_{12}$	$-S_{11}$	$-S_{22}$
CFRE	67.6	67.6	4.2	4.2	0.04	885	885	97	835	835

Table 4. Mechanical properties of carbon fibre lamina, as provided by the manufacturer.

2.2. Specimen preparation and tensile test conditions

In this investigation, six types of joint configurations are tested and analysed with experiments with possible combinations of AA 2024-T3 substrates with AA 2024-T3 and CFRE doublers joined under riveted, bonded or hybrid conditions. Fabricated lap joints are tested under static load to determine their strength. Fig. 3 shows lap joint configurations of AA 2024-T3 substrates with AA 2024-T3 and CFRE doublers under riveted, bonded and hybrid conditions. Specimens are designed and prepared in accordance with the FAA regulations mentioned in chapter 4 of aviation maintenance technician hand book-airframe [48]. According to these standards, the minimum rivet pitch should be 3 rivet diameters and usually, an average rivet pitch ranges from 4 to 6 rivet diameters with an edge distance of 2 to 2.5 rivet diameters. Riveted specimens in this study have rivet pitch of 5.3 rivet diameters with an edge distance of 2.5 rivet diameters. All the specimens comply with the standards set by FAA. Three specimens of each type of joint configurations are tested, with a total of eighteen experiments. Holes of 5 mm in diameter are drilled in substrates and doublers for positioning rivets during the fabrication of riveted and hybrid specimens. Riveted specimens comprised of eight rivets in a single row with rivet pitch of

25.4 mm. A pop rivet gun was used to squeeze the rivets in riveting process. In this investigation, the performance of riveted lap joint is compared with bonded and hybrid lap joints. Hence, the dimensions of substrate and doublers for bonded and hybrid lap joints are same as riveted lap joint.

A thin uniform layer of Araldite 2031 is applied between surfaces of substrate and doublers in preparation of bonded and hybrid joints. Bonded specimens are cured for 16 hours at 40^0C to achieve high performance of adhesive. Post curing, rivets are fastened to the bonded specimens to prepare hybrid joints.

All specimens are subjected to tensile loading using a Metrotest 810 testing machine. The testing system is controlled by a computer, installed with Metrotest software tool. Static tests are performed at displacement control rate of 6 mm/min. Crosshead displacement and load are recorded throughout the test at a sampling rate of 10 readings per second.

Fig. 3. Riveted (1, 4), bonded (2, 5) and hybrid (3, 6) specimens with AA 2024-T3 substrates and with AA 2024-T3 doublers (left) or carbon fibre reinforced epoxy (CFRE) doublers (right)

2.3. Numerical modelling

Numerical analysis is performed on six lap joint configurations using 3D finite element models created and analysed in commercial finite element code ABAQUS. Substrate and doublers are modelled as shell elements. Shell elements provided optimised solution between a number of elements and computation time with good accuracy. Metal substrates, doublers and composite doublers are modelled as shell elements with 4-node doubly curved thin shell (S4R) with reduced integration. Static analysis of six joint configurations is performed using a dynamic implicit algorithm to obtain load-displacement curves and stress distribution on substrate and doublers. Quad-dominated medial axis meshing is used in meshing shells and medial axis meshing provided uniform mesh distribution of substrates and doublers. The dynamic implicit algorithm has least

convergence issues compared to general algorithm and results are in good agreement with experiments. All the models are symmetrical; hence, symmetry boundary condition is used for obtaining load-displacement curves and stress analysis. A half model of the joint was analysed for each case to increase efficiency by reducing computational time with detailed mesh. Surface to surface contact algorithm is used to generate contact interfaces between substrates and doublers. Contact interactions are considered as frictionless and hard contact with no penetration. An element size of 1 mm is considered for all models with substrate comprised of 4275 elements, doubler 1 and doubler 2 have 2700 and 2075 elements, respectively. All the lap joint models are loaded similar to experimental conditions. An equation constraint is created using a set of follower nodes (all nodes except load node) tied to load node (a single node) on the edge. Load-displacement values for different models are obtained from single load node. When the load is applied to load node, all follower nodes will experience the same boundary condition. Hence, computing values at load node provide response of overall joint. A detailed stress analysis is performed on all models with the same mentioned modelling technique.

According to FAA regulations, repairs are mandatory for structures with a crack length of 12.7 mm, but in real-case, it is possible to reinforce the damaged/cracked structure before reaching the regulation limit. Hence, numerical analysis is performed on un-reinforced and reinforced cracked metal substrate with metal and composite doublers. SIFs are computed for substrates for crack lengths of 1, 5 and 10 mm. Cracked metal substrates are reinforced with metal and composite doublers under riveted and bonded condition. Investigation on SIFs provided the effectiveness of reinforcements under riveted and bonded configurations compared to the un-reinforced cracked substrate. For numerical analysis of un-reinforced and reinforced cracked substrate, the dynamic explicit algorithm is used for computing SIFs. Material properties used in the numerical analysis are presented in Tables 1, 3 and 4.

2.3.1. Rivet modelling

Rivets can be modelled in different methods as presented in Ref. [18]. In this study, rivets are modelled as point-based fasteners. Properties of the rivets are considered as bushing elements with stiffness in six degrees of freedom (DOF): three in translational and three in rotational directions. Stiffness in translational and rotational directions of bushing elements are calculated using the equations 1-5 [49]. A radius of influence 2.5 mm is considered for fasteners with a continuum distribution of properties of fasteners.

$$K_1 = \left\{\frac{k}{m}\left[\left(\frac{t_{shell1}+t_{shell2}}{2d}\right)^{\lambda}\left(\frac{1}{E_{11,shell1}t_{shell1}}+\frac{1}{m.E_{11,shell2}t_{shell2}}+\frac{1}{2.E_{fast}t_{shell1}}+\frac{1}{2m.E_{fast}t_{shell2}}\right)\right]\right\}^{-1} \quad \text{Eq. (1)}$$

$$K_2 = \left\{\frac{k}{m}\left[\left(\frac{t_{shell1}+t_{shell2}}{2d}\right)^{\lambda}\left(\frac{1}{E_{22,shell1}t_{shell1}}+\frac{1}{m.E_{22,shell2}t_{shell2}}+\frac{1}{2.E_{fast}t_{shell1}}+\frac{1}{2m.E_{fast}t_{shell2}}\right)\right]\right\}^{-1} \quad \text{Eq. (2)}$$

$$K_3 = \frac{\pi d^2 E_{fast}}{4(t_{shell1}+t_{shell2})} \quad \text{Eq. (3)}$$

$$K_4 = K_5 = \frac{\pi d^2}{16}\left(\frac{E_{fast}d^2}{4L}+G_{fast}.L\right) \quad \text{Eq. (4)}$$

$$K_6 = \frac{G\pi d^4}{32L} \quad \text{Eq. (5)}$$

where k is 2.2 and λ is 0.4 for solid rivets, m is 1 for single shear, t_{shell1} and t_{shell2} are the thicknesses of shell 1 and shell 2, d is the diameter of the rivet holes, E_{11}, E_{22} and E_{fast} are the elastic moduli of the metallic and composite plates and the fastener, respectively, G_{fast} is the shear modulus of the fastener, and L is the length of the fastener. The first rivet row has a shell thickness 1 of 3.175 mm (substrate) and a shell thickness 2 of 1.5875 mm (doubler 1). Second, third and

fourth rivet rows have shell thickness 1 of 3.175 mm (substrate) and shell thickness 2 of 3.175 mm (doubler 1 and doubler 2).

2.3.2. Adhesive modelling

The adhesive bond between the substrate and doublers is modelled by generating a cohesive contact interface. This interface has no physical thickness, but properties for cohesive contact are calculated for the thickness of 0.25 mm. Cohesive contact algorithm is used to model the interaction between surfaces. This algorithm uses linear elastic traction-separation behaviour to simulate adhesive behaviour. Traction-separation criteria provide good accuracy with low error margin compared to experiments [38]. Traction-separation model used in ABAQUS assumes initially a linear elastic behaviour, followed by damage initiation and evolution. Elastic behaviour of cohesive elements is described in terms of nominal stresses and nominal strains across the interface. Nominal stresses are force components divided by area at each integration point. Nominal stress vector consists of three components t_n, t_s and t_t (n represents normal the direction and s and t represents shear and traction directions) and corresponding nominal separations are δ_n, δ_s and δ_t. Nominal strains are defined as nominal separations divided by the original thickness of the cohesive element T_0 shown in Eq. 6.

$$\varepsilon_n = \frac{\delta_n}{T_0}, \varepsilon_s = \frac{\delta_s}{T_0} \text{ and } \varepsilon_t = \frac{\delta_t}{T_0} \qquad \text{Eq. (6)}$$

Elastic behaviour of cohesive elements is written as

$$t = \begin{Bmatrix} t_n \\ t_s \\ t_t \end{Bmatrix} = \begin{bmatrix} k_{nn} & k_{ns} & k_{nt} \\ k_{sn} & k_{ss} & k_{st} \\ k_{tn} & k_{ts} & k_{tt} \end{bmatrix} \begin{Bmatrix} \varepsilon_n \\ \varepsilon_s \\ \varepsilon_t \end{Bmatrix} = K\varepsilon$$

In this study, uncoupled behaviour between traction and separation is used, so the off-diagonal terms are zero in the elasticity matrix K. Properties of adhesive are calculated in terms of stiffness k_{nn}, k_{ss} and k_{tt}, where k_{nn} is Young's modulus of adhesive divided by thickness T_0 and k_{ss} and k_{tt} are the shear modulus of adhesive divided by the thickness T_0.

Damage of adhesive is modelled with progressive failure of the cohesive elements which is defined in terms of traction-separation response. Failure mechanism consists of three stages: damage initiation, damage evolution. The initial response of cohesive elements is linear and once damage initiation criterion is met, damage evolution occurs according to the damage evolution law. Fig. 4 shows the traction-separation response with failure mechanism.

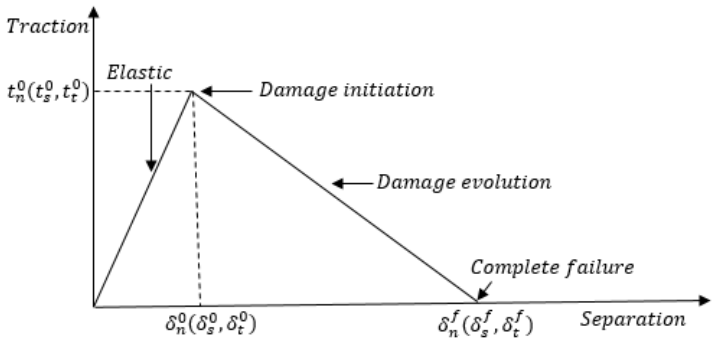

Fig. 4. Traction-separation response with the failure mechanism

Damage initiation begins when the cohesive elements reach specified criterion. In this case, quadratic nominal stress criterion is considered for initiation criterion and for Araldite 2031 it is 25 MPa (data provided by the supplier). Damage is initiated when nominal stress ratios in quadratic interaction function reach a value of 1. Eq. 7 represents the quadratic nominal stress criterion

$$\left\{\frac{\langle t_n \rangle}{t_0^n}\right\}^2 + \left\{\frac{t_s}{t_0^s}\right\}^2 + \left\{\frac{t_t}{t_0^t}\right\}^2 = 1 \qquad \text{Eq. (7)}$$

For deformations purely normal to the interface, the terms t_0^n, t_0^s and t_0^t are peak values of nominal stress. The term $\langle t_n \rangle$ signifies that no damage is initiated if the deformation is compressive of nature.

Once damage initiation begins, damage evolution takes place in the cohesive elements. Hence, a damage evolution law describes the rate of degradation of cohesive elements. A scalar damage quantity D represents the overall damage of the cohesive elements. The quantity D ranges from 0 to 1: $D = 0$ represents that no damage has occurred in the cohesive elements and $D = 1$ represents a complete damage of the elements. Damage in the traction-separation model consists of stress components (t_n, t_s and t_t) shown in Eq. 8, 9 and 10.

$$t_n = \begin{cases} (1-D)\bar{t}_n, & \bar{t}_n \geq 0 \\ \bar{t}_n \; otherwise\,, \end{cases} \qquad \text{Eq. (8)}$$

$$t_s = (1-D)\,\bar{t}_s, \qquad \text{Eq. (9)}$$

$$t_t = (1-D)\,\bar{t}_t \qquad \text{Eq. (10)}$$

Terms $\bar{t}_n, \bar{t}_s$ and $\bar{t}_t$ are stress components for the current strains without damage as predicted by elastic traction-separation behaviour.

In this study, damage evolution is based on the energy dissipated as a result of a damaging process called fracture energy. Fracture energy is the area under the traction-separation curve. Araldite 2031 has a fracture energy of $2\ kJ/m^2$ (provided by the manufacturer) with linear softening behaviour and fracture toughness of $1.6MPa \cdot m^{1/2}$.

3. Results and Discussion

3.1 Experimental results

Load-displacement curves measured for metal-metal and metal-composite configurations of riveted, bonded and hybrid joints are shown in Fig. 5a and 5b. Table 5a and 5b show the strength of each type of joint for tested specimens with average strength and standard deviation. Failure modes of the joints are independent of whether the joints are mechanically fastened or purely bonded or hybrid joints.

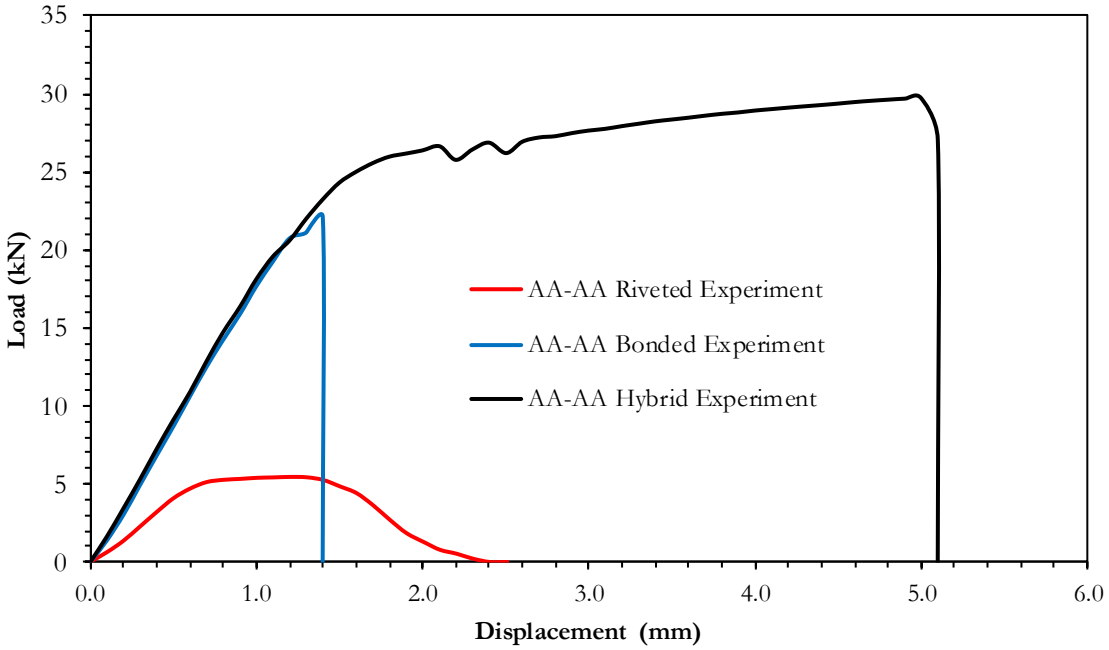

Fig. 5a. Load vs. displacement curves measured for riveted, bonded and hybrid joint configurations of AA 2024-T3 substrate–AA 2024-T3 doublers.

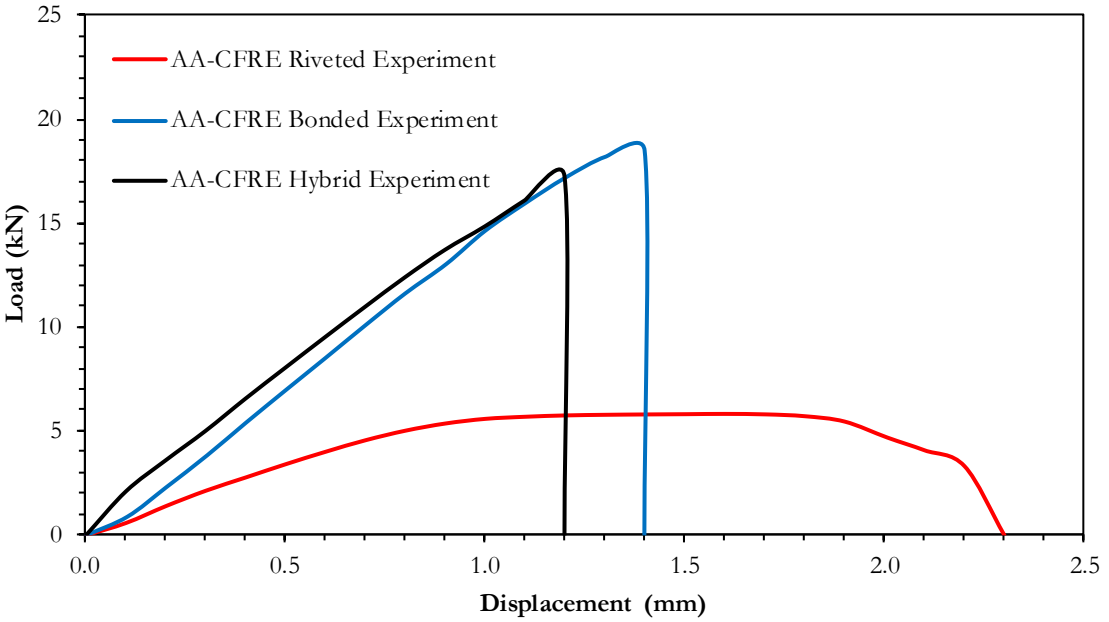

Fig. 5b. Load vs. displacement curves measured for riveted, bonded and hybrid joint configurations with AA 2024-T3 substrate–CFRE doublers.

Joint Configuration	AA 2024T3-AA2024 T3				
	Strength of Specimen 1 (kN)	Strength of Specimen 2 (kN)	Strength of Specimen 3 (kN)	Average Strength (kN)	Standard Deviation (kN)
Riveted Joint	5.4	5.4	5.5	5.4	0.06
Bonded Joint	22.1	26.0	21.0	23.0	2.6
Hybrid Joint	29.3	29.7	26.0	28.3	2.0

Table 5a. Joint strength for riveted, bonded and hybrid joint configurations with AA 2024-T3 substrate–AA 2024-T3 doublers

Joint Configuration	AA 2024T3-CFRE				
	Strength of Specimen 1 (kN)	Strength of Specimen 2 (kN)	Strength of Specimen 3 (kN)	Average Strength (kN)	Standard Deviation (kN)
Riveted Joint	5.8	6.0	5.9	5.8	0.1
Bonded Joint	22.5	18.5	17.3	19.4	2.7
Hybrid Joint	17.3	17.8	15.0	16.7	1.5

Table 5b. Joint strength for riveted, bonded and hybrid joint configurations with AA 2024-T3 substrate–CFRE doublers.

AA 2024-T3–AA 2024-T3 (metal-metal) riveted lap joint failed at peak load of 5.4 kN with a displacement of 1.3 mm. The displacement of 1.3 mm is due to the rivets shear and no plasticity is observed in substrate or doublers. Failure mode in metal-metal riveted lap joint is pure rivet shear and failure of the joint is due to complete failure of rivets at the bottom substrate (Fig. 6 left). From Fig. 5a, the load-displacement curve can be split into two parts: elastic and plastic. Joints behaved elastic up to 4 kN and yielded above this load. It can be said from the experimental result that limit load (ultimate load/factor of safety) for metal-metal riveted joint is 3.6 kN, when a safety factor 1.5 is applied. Each rivet carried a load of 1.36 kN, which is also called rivet value. The standard deviation of 0.06 kN is observed in the strength of these specimens.

A similar type of failure mode is observed in AA 2024-T3–CFRE (metal-composite) riveted joint (Fig. 6 right), but this joint failed at slightly higher load than metal-metal riveted joint (at peak load of 5.8 kN with 1.8 mm displacement). Metal-composite joint behaved elastic up to 4.2 kN with a rivet value of 1.46 kN and carried 6.9% more load than metal-metal riveted joint. This difference is due to the higher stiffness of composite doublers compared to metal doublers, which affects the load transfer between substrate and doublers. Because of the high stiffness of composite doublers, slightly higher yield of aluminium rivets is observed for metal-composite riveted lap joint compared to metal-metal riveted lap joint. Calculated limit load for riveted metal-composite lap joint is 3.9 kN with a standard deviation of 0.1 kN for specimens' strength.

Fig. 6. Rivet shear failure of AA 2024-T3–AA 2024-T3 (left) and AA 2024-T3–CFRE (right) riveted joints

The behaviour of pure adhesively bonded metal-metal and metal-composite joints is different compared to pure riveted joints. Pure adhesive bonded joints are stiffer with a higher

slope in the elastic zone of the load-displacement curves (Fig. 5a and Fig. 5b). Pure bonded joint carried a higher load than pure riveted joints. The bonded metal-metal joint has an average strength of 23 kN with a displacement of 1.4 mm. Since there is no presence of yield, the joint has failed abruptly upon reaching the failure load. Adhesive failure is observed as the failure mode of this joint (Fig. 7 left). With a factor of safety 1.5, the calculated limit load for the safe operation of the pure bonded metal-metal joint is 15.3 kN, and standard deviation of 2.6 kN is observed in the strength of these specimens. Bonded area and adhesive used for both metal-metal and metal-composite joints are the same, but the latter has 15.9% lower average strength compared to the pure bonded metal-metal joint; particularly, 19.4 kN with a displacement of 1.4 mm. The difference in strength may be due to the fact that the load transfer between metal-metal is higher through the adhesive layer. The failure mode for pure bonded metal-composite joint is due to adhesive failure with all the adhesive attached to the substrate. Secondary bending is observed in pure bonded metal-metal joints (Fig. 7 right), which may be due to higher thickness of substrate and doublers in these joints. A standard deviation of 2.7 kN is observed for pure bonded metal-composite joint with a calculated limit load capacity of 12.9 kN.

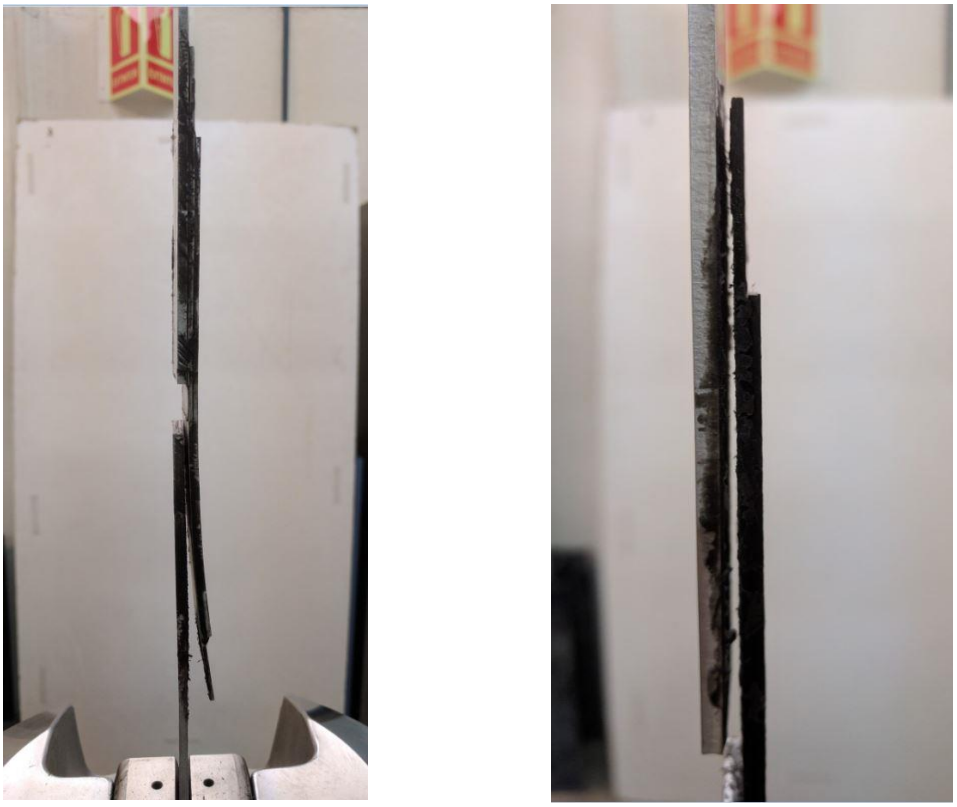

Fig. 7. Adhesive failure of AA 2024-T3–AA 2024-T3 (left) and AA 2024-T3–CFRE (right) bonded joints

Load-displacement curves of hybrid metal-metal and metal-composite joints are shown in Fig.5a and Fig. 5b. The former has the highest average strength of all studied joint configurations (28.3 kN, with failure at the displacement of 5.1 mm). Interestingly, yield behaviour is observed for the hybrid metal-metal joint. The standard deviation in strength for these samples is 2.0 kN. Adhesive failure and rivet shear (Fig. 8 left) are observed in the failure of hybrid metal-metal joint with a safe limit load of 18.9 kN. In particular, failure occurred in two stages: initial adhesive failure and finally rivet shear. Hybrid metal-composite joint has similar load-displacement behaviour compared to the bonded metal-composite joint. The former has 41% lower strength than hybrid metal-metal joint, which is a significant difference. The average strength of the hybrid metal-

composite joint is 16.7 kN with a displacement of 1.2 mm. No yield is observed for the hybrid metal-composite joint when compared to the hybrid metal-metal joint. The standard deviation of 1.5 kN is observed for the hybrid metal-composite joint. The failure mode of this joint is due to net-section failure of doublers (Fig. 8 right). Doublers have failed close to the rivet row which is closest to the crack edge. Net-section failure suggests that composite doublers are much stiffer than aluminium alloy metal doublers, but, when holes are present in composite doublers, their strength deteriorates by 11% compared to their strength without holes (pure bonded joints). Secondary bending is observed only for hybrid metal-metal joint and this is due to the higher thickness of substrate and doublers. From the works presented in Ref. [27], the hybrid joint configuration of composite-composite double lap joint has performed better compared to riveted and bonded configurations under static and fatigue loading.

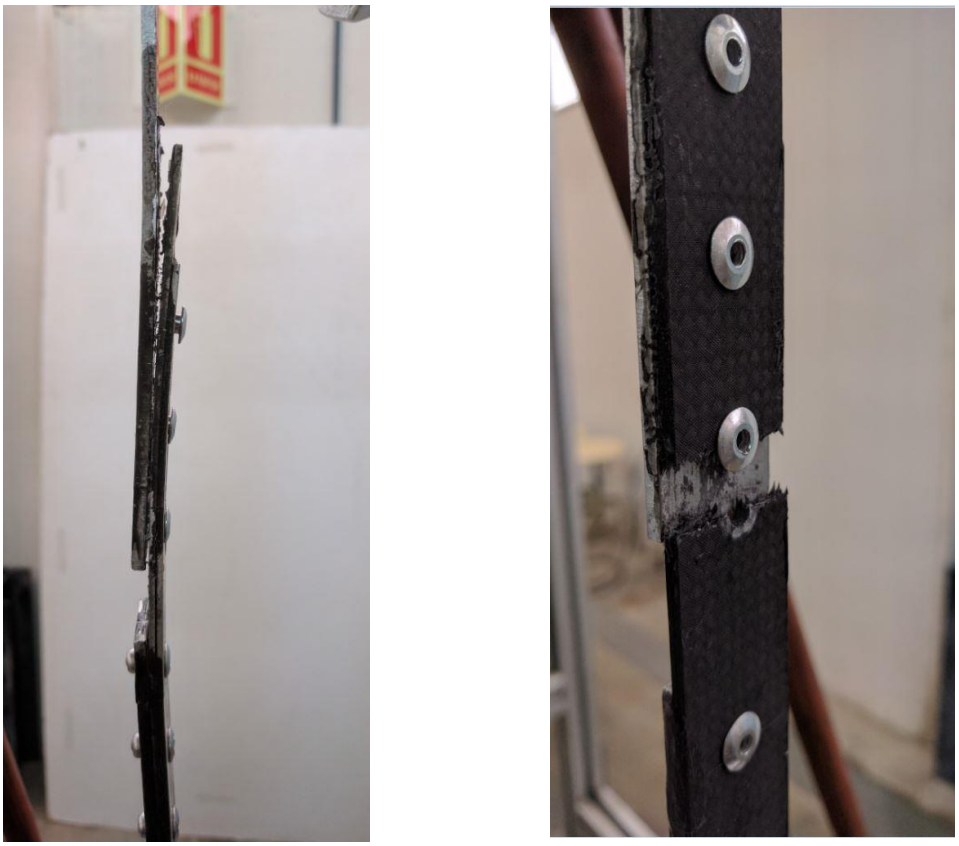

Fig. 8. Hybrid joint failure of AA 2024-T3–AA 2024-T3 (left) and AA 2024-T3–CFRE (right) hybrid joints.

Table 6 shows comparison of average strengths of lap joints in relative percentages. Lap joint configurations of columns of the table are compared with lap joint configurations of rows. For example, the average strength of bonded AA 2024-T3–AA 2024-T3 is 423% of the average strength of riveted AA 2024-T3–AA 2024-T3 configuration. From the table, it can be noticed that the hybrid metal-metal lap joint has the highest average strength and that repairs of metal substrates with adhesive bonding are the most suitable. Despite high standard deviation of adhesive joints, hybrid joints are advantageous with rivets providing an additional level of protection in case of premature or early adhesive failure.

Joint configuration		AA 2024-T3–AA 2024-T3			AA 2024-T3–CFRE		
		Riveted	Bonded	Hybrid	Riveted	Bonded	Hybrid
AA 2024-T3–AA 2024-T3	Riveted	X	423%	519%	107%	355.7%	305.5%
	Bonded	24%	X	123%	24%	84%	72%
	Hybrid	19%	82%	X	19%	69%	59%
AA 2024-T3–CFRE	Riveted	94%	396%	485%	X	333%	286%
	Bonded	28%	119%	146%	30%	X	86%
	Hybrid	33%	138%	170%	35%	116%	X

Table 6. Comparison table of average strengths of AA 2024-T3–AA 2024-T3 and AA 2024-T3–CFRE lap joints under riveted, bonded and hybrid configurations.

3.2 Numerical analysis results

3.2.1 Load-displacement curves

Load-displacement curves for lap joints of metal-metal and metal-composite under riveted, bonded and hybrid conditions are obtained numerically using finite element code ABAQUS. Fig. 9a, 9b and 9c show, for pure riveted, pure bonded and hybrid joints, respectively, the experimental and numerical load-displacement curves of metal-metal and metal-composite.

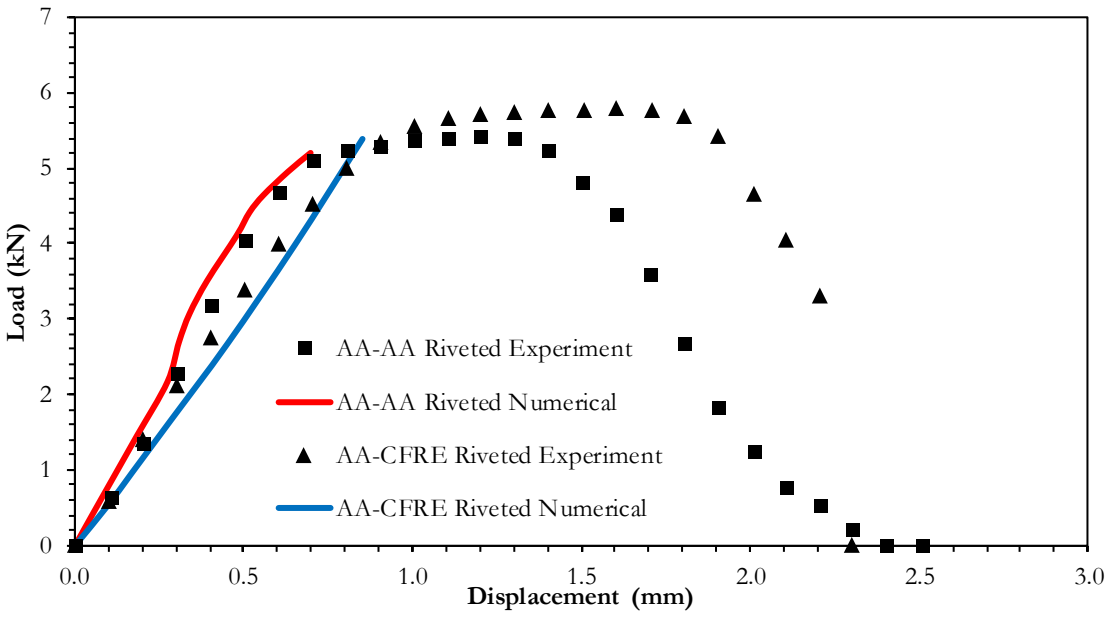

Fig. 9a Experimental and numerical load-displacement curves for riveted metal-metal and metal-composite lap joints.

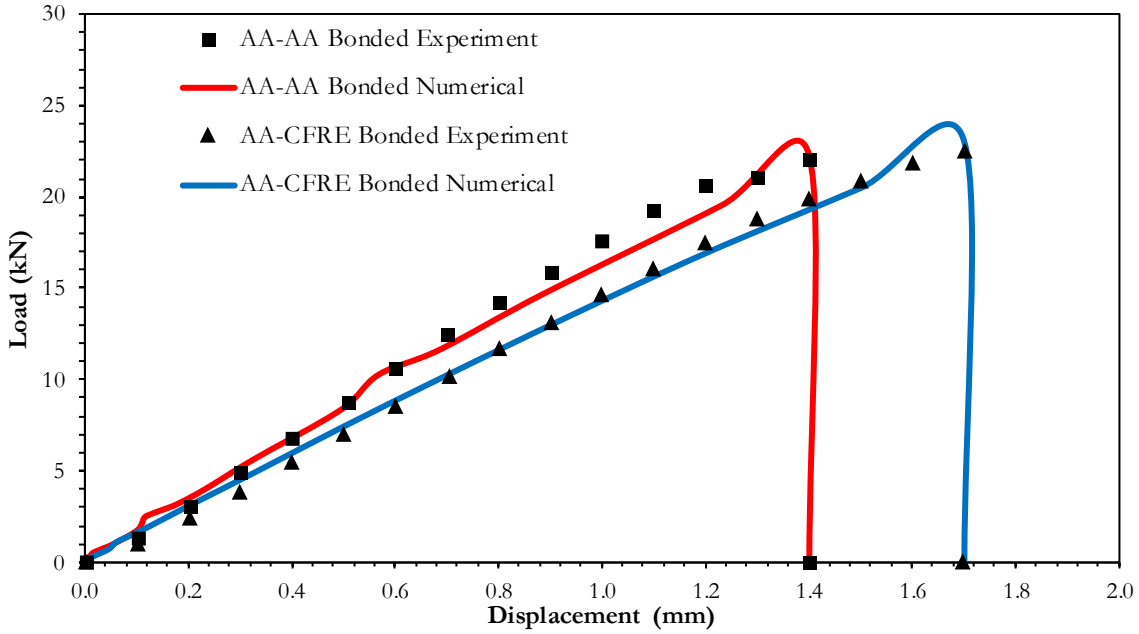

Fig. 9b Experimental and numerical load-displacement curves for bonded metal-metal and metal-composite lap joints.

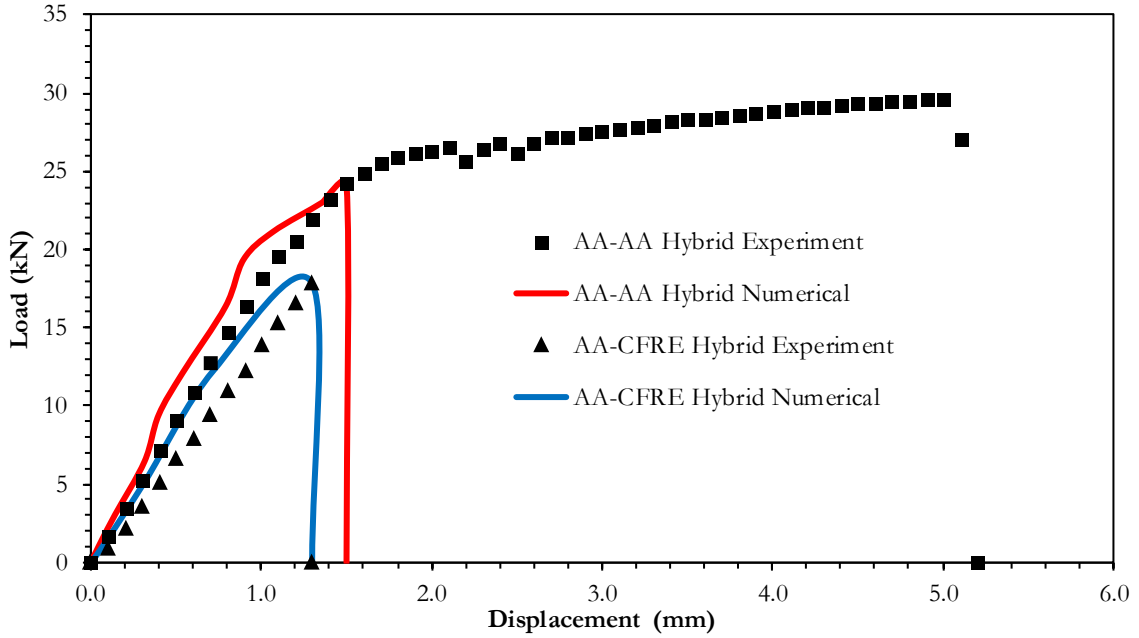

Fig. 9c Experimental and numerical load-displacement curves for hybrid metal-metal and metal-composite lap joints.

Rivets in the riveted and hybrid joints are modelled as point-based fasteners with a radius of influence of 4.75 mm. Effects of compression and plasticity in the rivet modelling are not considered for point-based fasteners. This approach is closer to the practice in the aviation industry, as there are numerous fasteners in the structure, hence point-based fasteners are a quick and reliable way of modelling rivets. Table 7 shows difference between numerical strength and average experimental strength for various joint configurations. The difference in numerical and average experimental strengths for riveted metal-metal and metal-composite lap joint is 1.9% and 1.9%, respectively. Cohesive contact interface for bonded and hybrid joints are modelled and

simulated with similar conditions to experimental samples. From Fig. 9b, a difference of 0.9% is observed between numerical and average experimental strength of metal-metal bonded lap joint. A slightly higher difference (2.2%) is observed for bonded metal-composite. Hybrid joints of metal-metal and metal-composite are modelled using both point-based fasteners and cohesive contact interface. For the models of hybrid metal-metal and hybrid metal-composite lap joints, average experimental strength is higher by 0.4% and 0.6% than numerical strength.

Joint Configuration		Numerical Strength (kN)	Average Experimental Strength (kN)	% difference
AA 2024-T3–AA 2024-T3	Riveted Joint	5.2	5.1	1.9%
	Bonded Joint	22.2	22.0	0.9%
	Hybrid Joint	24.2	24.3	-0.4%
AA 2024-T3–CFRE	Riveted Joint	5.4	5.3	1.9%
	Bonded Joint	23.0	22.5	2.2%
	Hybrid Joint	17.9	17.8	-0.6%

Table 7. Strengths obtained in numerical analysis and experiments, and the percentage difference between numerical and experimental values.

3.2.2 Numerical Stress Analysis

A detailed stress analysis is performed on metal-metal and metal-composite lap joints of riveted, bonded and hybrid joint configurations. As discussed in experimental results, a safety factor of 1.5 is applied to aircraft structures in the aviation industry to ensure safety during operation. In this investigation, the limit load of riveted metal-metal lap joint is applied as a boundary condition for the other joint configuration models, and stresses are computed at specific locations shown in Fig.10a. These locations are the mid-points in between each rivet row starting from first rivet row to fourth rivet row on substrate and doublers.

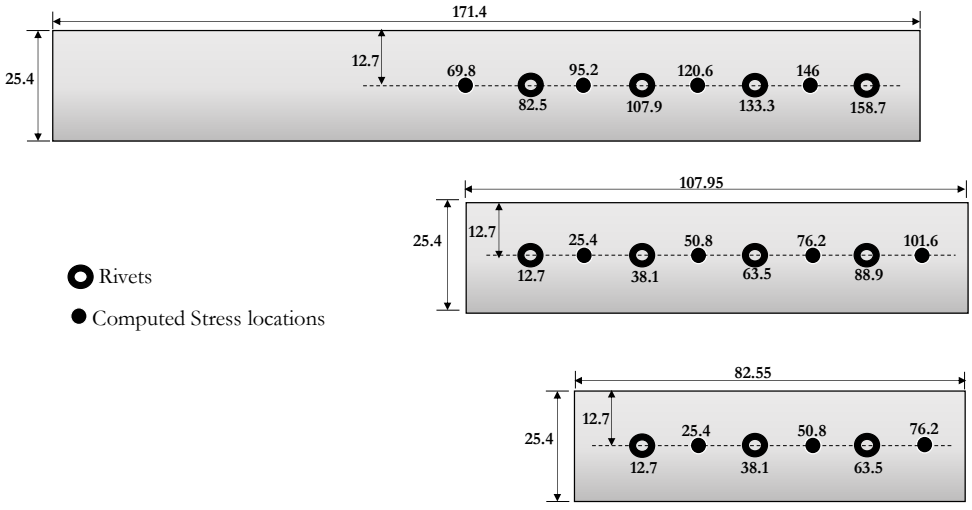

Fig. 10a. Locations at which Von-Misses stresses are computed in finite element analysis (FEA) on substrate (top), doubler 1 (middle) and doubler 2 (bottom). (All dimensions are in mm).

Models of riveted metal-metal and metal-composite for detailed stress analysis are modelled with holes on substrate and doublers as shown in Fig. 10b. Point-based fasteners do not provide stresses around the holes, so rivets are modelled using multiple point constraints (MPCs) discussed in Ref. [18]. MPCs are connected to the reference points on top and bottom surface of substrate and doublers. Top and bottom reference points are connected using wire feature with bushing elements in six DOF. The stiffness of bushing elements is calculated using Eq. 1-5. Bonded models are similar to riveted models, but no holes are present on substrate and doublers. Von-Misses stresses are computed at element locations on substrate and doublers, as shown in Fig. 10a.

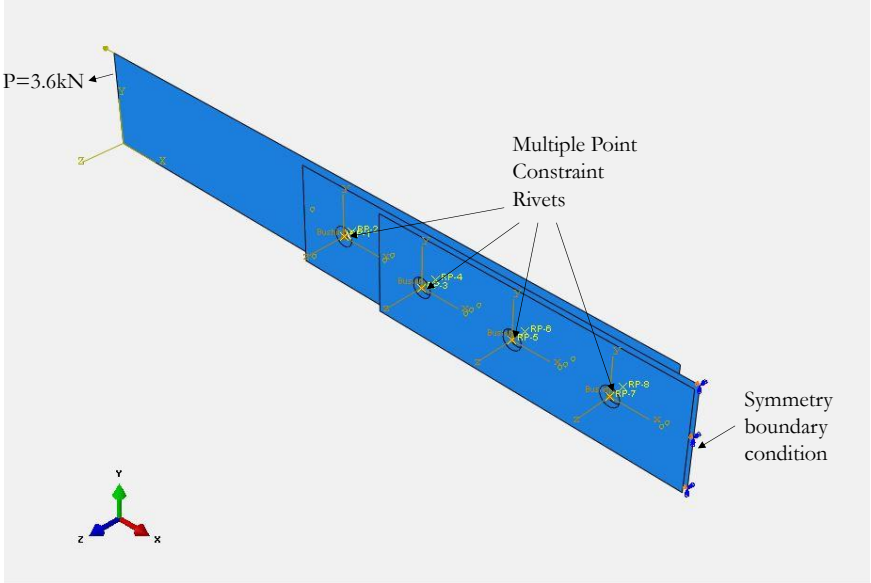

Fig. 10b. Finite element model of the riveted lap joint for detailed stress-analysis.

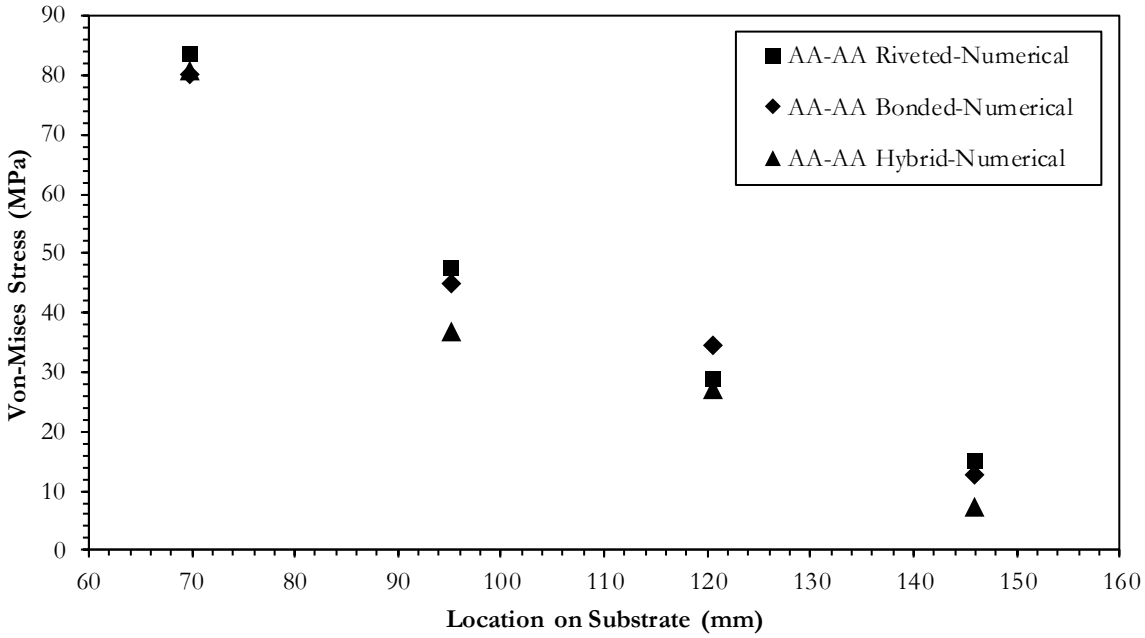

Fig. 11a. Von-Misses stress on AA 2024 T3 substrate with AA 2024 T3 doublers for riveted, bonded and hybrid joints.

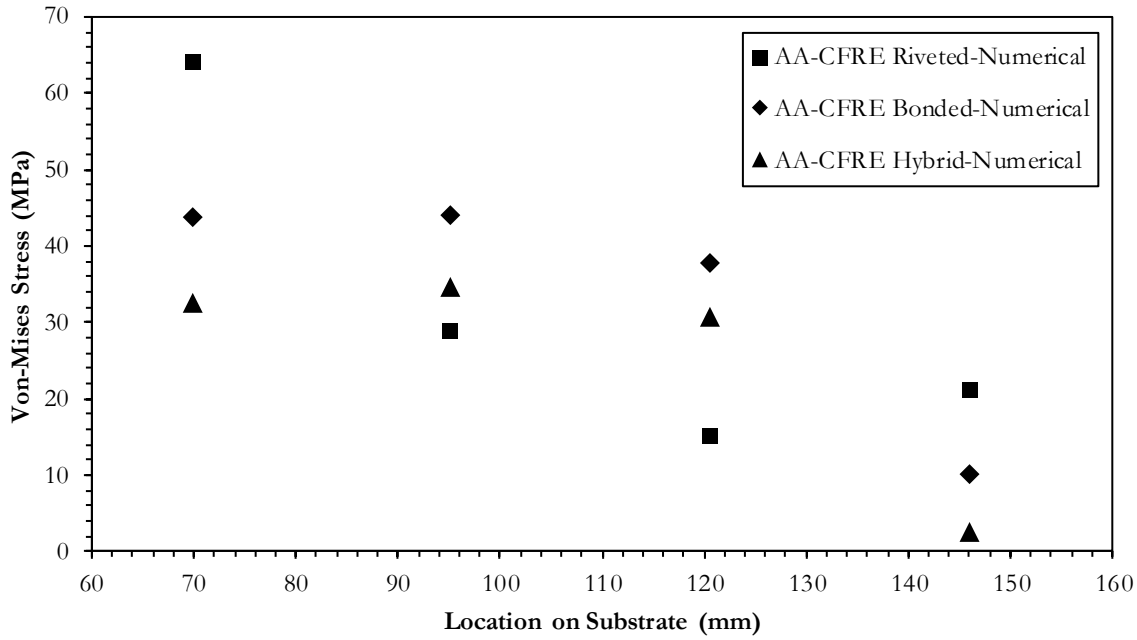

Fig. 11b. Von-Misses stress on AA 2024 T3 substrate with CFRE doublers for riveted, bonded and hybrid joints.

Riveted, bonded and hybrid configurations of metal-metal lap joints have a nearly same value of Von-Misses stress (80 MPa) at location 69.8 mm. From the location 69.8 mm to 146 mm, a reduction in Von-Misses stress is observed (Fig. 11a). Reduction of Von-Misses stress across the substrate is influenced mainly due to load transfer between substrate and doublers. The hybrid joint has the lowest value at 146 mm which is 56.6% (47.4%) of bonded (riveted) joint Von-Misses stress.

In case of metal-composite lap joints, a different pattern is observed (Fig. 11b): Von-Misses stresses for riveted, bonded and hybrid joints at location 69.8 mm are lower compared to metal-metal lap joint configurations. This may be due to the higher stiffness of composite doublers compared to metal doublers. Hence, this affects the load transfer between substrate and doublers. Among metal-composite lap joint configurations, riveted configuration at 69.8 mm has highest Von-Misses stress, which is nearly 1.5 times that of bonded joint, and twice of the hybrid joint. From location 69.8 mm to 120.6 mm, riveted metal-composite lap joint showed a decrease in Von-Misses stress with a sudden increase observed at location 146 mm, closest to crack edge. This behaviour can be due to high load transfer between the first, second and third rivet rows, hence lowering the stresses on the substrate. Lowest Von-Misses stress is observed for the hybrid joint at 146 mm, which is due to efficient load transfer by adhesive and rivets compared to just rivets or adhesive. For same boundary conditions, hybrid joints have 4 times lower Von-Misses stress to bonded joints on the substrate at 146 mm.

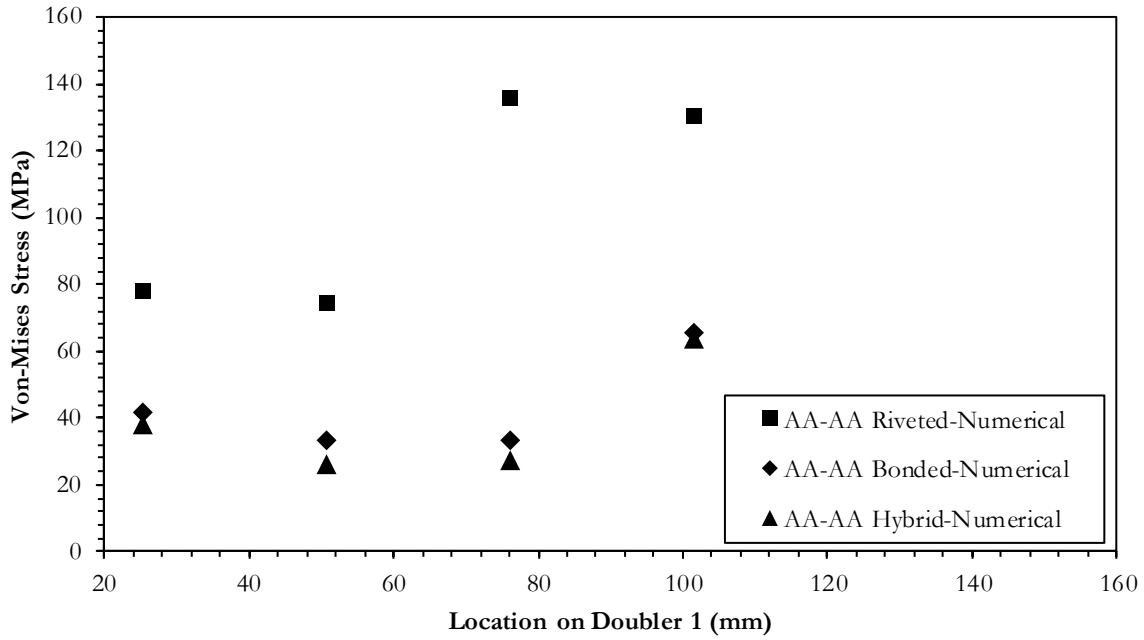

Fig. 12a. Von-Misses stress on doubler 1 of AA 2024 T3 substrate with AA 2024 T3 doublers under riveted, bonded and hybrid joints.

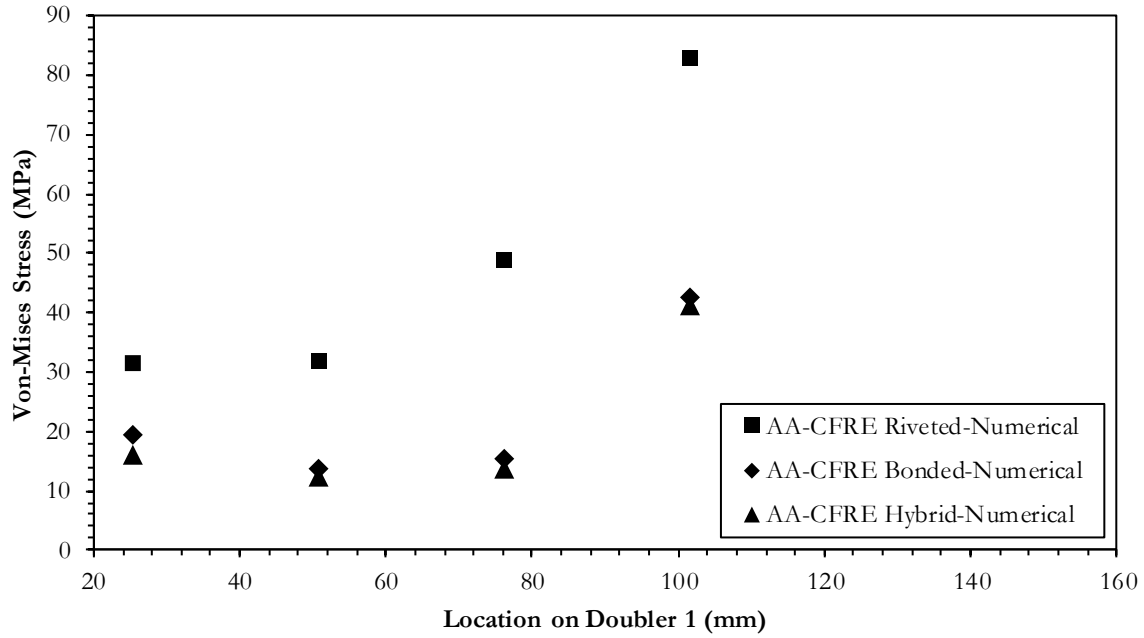

Fig. 12b. Von-Misses stress on doubler 1 of AA 2024 T3 substrate with CFRE doublers under riveted, bonded and hybrid joints.

Fig. 12a and 12b show Von-Misses stress on AA 2024-T3 and CFRE doubler 1 at 25.4, 50.8, 76.2 and 101.6 mm. Riveted lap joint shows highest Von-Misses stress in all locations for all configurations. The highest value of Von-Misses stress is observed at 76.2 mm, which is 1.7 times of value at 25.4 mm. From the Fig. 12a, it can be said that higher stresses on the riveted joint are due to high load transfer from substrate to doubler 1 through rivet rows. This may be the reason for low stresses observed on the substrate of the riveted joint compared to other configurations. Bonded and hybrid lap joints have a nearly same value of Von-Misses stress at all locations on doubler 1. For metal-composite joint configurations, Von-Misses stresses on doubler 1 are lower

compared to metal-metal joints. Von-Misses stresses for metal-metal and metal-composite lap joint configurations suggest composite doublers are better for smoother stress distribution with stresses half of metal doubler.

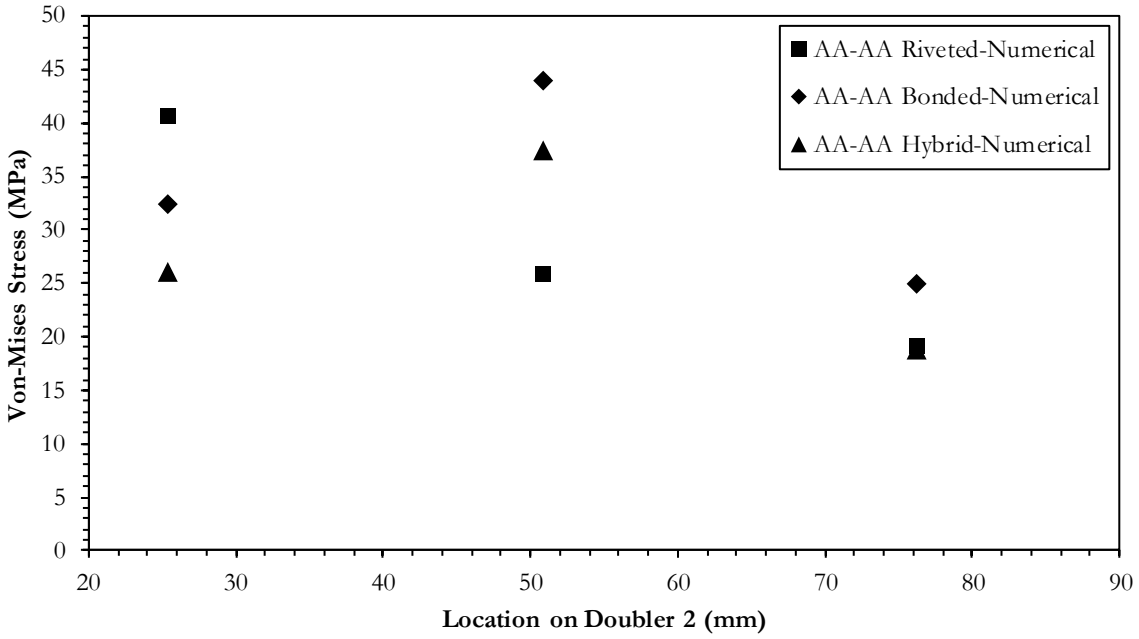

Fig. 13a. Von-Misses stress on doubler 2 of AA 2024 T3 substrate with AA 2024 T3 doublers under riveted, bonded and hybrid joints.

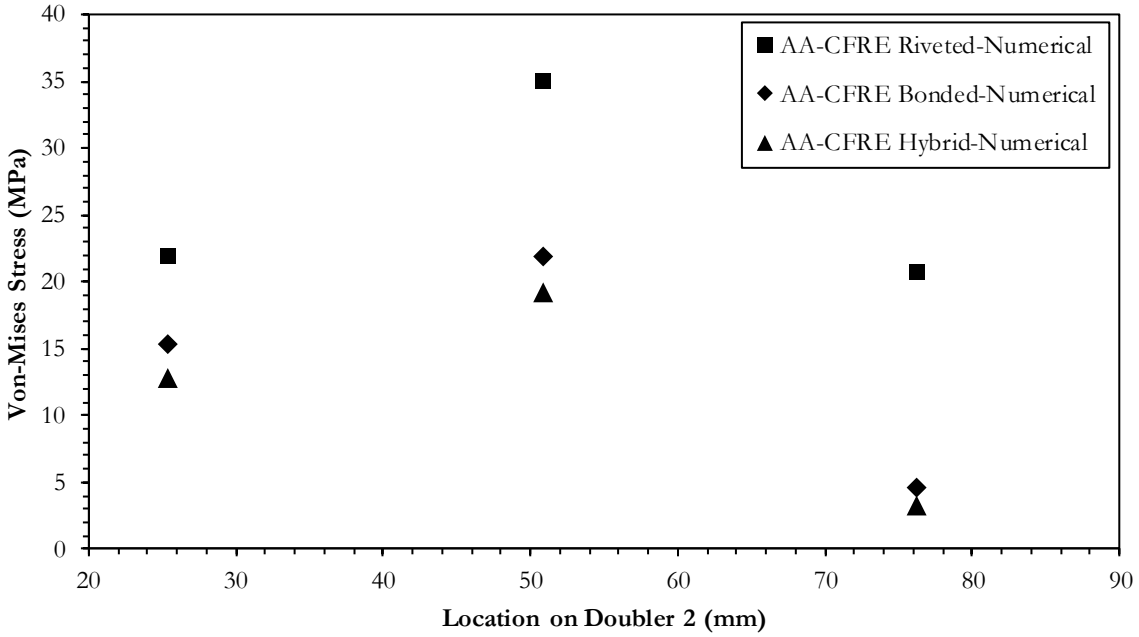

Fig. 13b. Von-Misses stress on doubler 2 of AA 2024 T3 substrate with CFRE doublers under riveted, bonded and hybrid joints.

Von-Misses stress for metal and composite doubler 2 at location 25.4, 50.8 and 76.2 mm is shown in Fig. 13a and 13b. At 25.4 mm on doubler 2, riveted joints of metal-metal and metal-composite shows highest Von-Misses stress. From (Fig. 13a) it is observed that stresses at 50.8 mm for bonded configuration are higher than other joints, this is due to high load transfer between doubler 1 to doubler 2 through the adhesive interface. Compared to metal doubler 2, composite

doubler 2 have lower Von-Misses stresses for riveted, bonded and hybrid joints. Von-Misses stress at 76.2 mm for composite doubler 2 is just 17% of metal doubler 2. This is due to the high stiffness of composite doublers compared to metal doublers which tend to have smooth load transfer paths between substrate and doublers.

3.2.3 Numerical analysis of reinforced cracked substrates

As discussed in the Materials and Methodology section, repairs/reinforcements can be performed on structures before critical crack length is reached. Thus, a numerical study is performed on reinforcement of cracked metal substrate for crack lengths of 1, 5 and 10 mm, which are lower than a critical crack length for full-repairs. Reinforcement is done under riveted and bonded conditions with metal and composite doublers of same dimensions as used in joint repairs studied previously. The analysis is performed on the hybrid configuration as well, but no difference in SIF's are found between bonded and hybrid joint. Hence, results of only riveted and bonded configuration are presented in this research. Contour-integral cracks are generated at the centre of the metal substrate shown in Fig. 14. Three models of metal substrate with 1, 5 and 10 mm cracks are reinforced with metal and composite doublers with similar boundary conditions: a load condition (force of 3.6 kN, which is the limit load of the riveted metal-metal joint) applied on the edges of the models with restricting forces/moments in other directions. Rivets are modelled as point-based fasteners and adhesive as cohesive contact with traction-separation criteria discussed in section 2.3.2.

Table 8 shows SIFs for un-reinforced and reinforced substrates with 1, 5 and 10 mm cracks for metal-metal and metal-composite configurations. From the table, it is significant that no difference is observed in SIFs for the substrate with the crack of 1 mm under riveted and bonded configuration. For the crack length of 5 mm, the SIFs for the substrate reinforced with riveted metal (composite) doublers are 12.7% (11.7%) lower than for the un-reinforced substrate. For the substrate reinforced with bonded metal (composite) doublers, the SIFs are 26.4% (22.3%) lower than for the un-reinforced substrate. For the crack length of 10 mm, the SIFs for the substrate reinforced with bonded metal and composite doublers are nearly 65% of the SIFs for the un-reinforced substrate. SIFs are 25.5% lower for bonded reinforcement compared to riveted reinforcement.

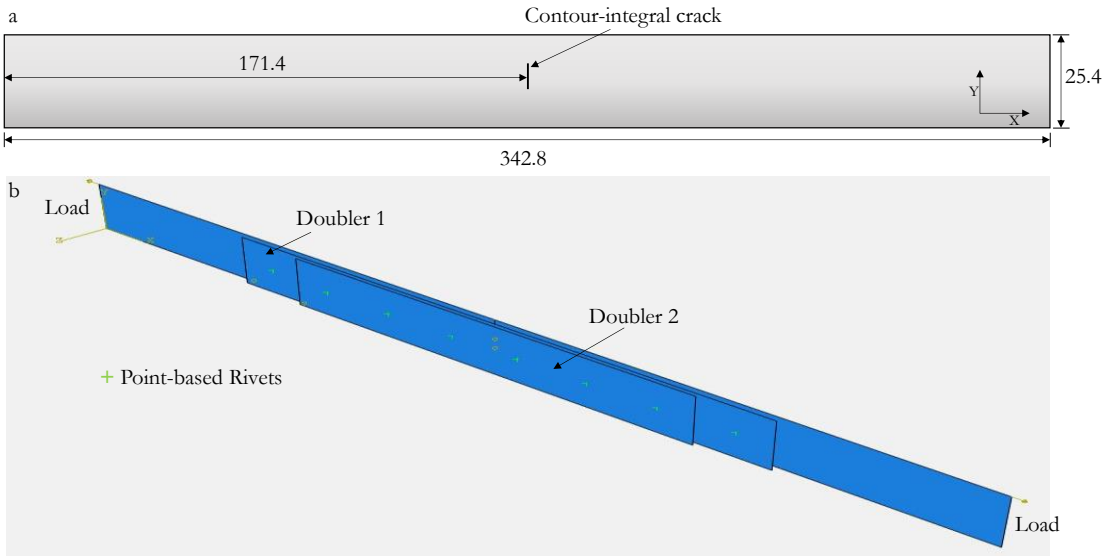

Fig. 14. (a) Cracked substrate with crack location (dimensions in mm), (b) Finite element model of the reinforced cracked substrate with point-based rivets.

Joint Configuration	SIFs for AA 2024-T3–AA2024-T3 (MPa·m$^{0.5}$)			SIFs for AA 2024-T3–CFRE (MPa·m$^{0.5}$)		
	Crack length (mm)			Crack length (mm)		
	1	5	10	1	5	10
Un-reinforced	1.76	4.02	6.16	1.76	4.02	6.16
Riveted reinforcement	1.55	3.51	5.33	1.57	3.55	5.42
Bonded reinforcement	1.52	2.96	3.95	1.55	3.12	4.04

Table 8. Stress intensity factors (SIFs) for un-reinforced and reinforced substrate for 1, 5 and 10 mm cracks for riveted and bonded joint configurations.

4. Conclusions

In this work, experimental results of riveted, bonded and hybrid repair lap joints of metal-metal and metal-composite are presented. Numerical analysis is performed and complemented to experimental results. A detailed numerical stress-analysis is performed on metal-metal and metal-composite joints to present stress distribution on substrate and doublers. Also, numerical analysis of un-reinforced and reinforced metal substrate with crack lengths 1, 5 and 10 mm, which are below critical crack length 12.7 mm according to FAR Part 25, are performed. Results obtained from this investigation lead to the following conclusions:

- Bonded metal-metal and metal-composite lap joints have nearly three times higher average strength than riveted metal-metal lap joint.
- Hybrid lap joints of metal-metal out-performed among all the lap joint configurations with 23% higher average strength than bonded metal-metal lap joint and 70% higher than metal-composite hybrid lap joint.
- Rivet shear caused failure in riveted lap joints, with each rivet carrying an average load of 1.36 kN for metal doublers and 1.46 kN for composite doublers.

- Bonded metal-metal and metal-composite lap joints failed due to adhesive failure. All the adhesive has remained on either substrate or doubler 1.
- Secondary bending is observed in bonded and hybrid metal-metal lap joints due to higher lap joint thickness. At failure, bending of doublers is observed (shown in Fig. 7 and 8 of metal-metal configuration).
- Failure in hybrid metal-metal lap joint occurred initially due to adhesive failure and later rivet shear. In case of hybrid metal-composite lap joint, net-section failure of doublers occurred close to the crack edge.
- Net-section failure of hybrid metal-composite joint showed the vulnerability of composite structures when plies are cut due to riveting process. Composite doublers are much stiffer than aluminium alloy metal doublers, but when there are holes in composite doublers their strength deteriorates by 11% compared to the strength without holes.
- Detailed stress analysis shows hybrid lap joints have low Von-Misses stresses on substrate and doublers.
- The cracked substrate with a crack length of 1 mm has no difference in SIFs for riveted and bonded doubler reinforcements.
- For the crack length of 10 mm, bonded reinforcement of metal or composite doublers to cracked substrates has 35% lower SIFs compared to the un-reinforced cracked substrate. Thus, bonded reinforcement reduces crack growth and improves the life of the cracked substrate.

5. Acknowledgements

This work was supported by MINECO grant FIS2017-82625-P and the Generalitat de Catalunya/AGAUR grant 2014 SGR 581. Mr Siddharth Pitta is also supported by the Generalitat de Catalunya/AGAUR FI grant 2017FI_B_00179. We would like to thank the valuable help provided by Francesc Joaquim Garcia, lab technician of Strength of Materials laboratory.

References

[1] L. Han, M. Thornton, M. Shergol, A comparison of the mechanical behaviour of self-piercing riveted and resistance spot welded aluminium sheets for the automotive industry. *Mater Des.* 31 (2010) 1457-1467.

[2] Y. Yan, W.D. Wen, F.K. Chang, P. Shyprykevich, Experimental study on clamping effects on the tensile strength of composite plates with a bolt-filled hole. *Compos. Part. A* 30 (1999) 1215–1229.

[3] R.H. Oskouei, M. Keikhosravy, C. Soutis, Estimating clamping pressure distribution and stiffness in aircraft bolted joints by finite-element analysis. *Proc. Inst. Mech. Eng. Part. G J. Aerosp. Eng.* 223 (2009) 863–871.

[4] J.M. Minguez, J. Vogwell, Effect of torque tightening on the fatigue strength of bolted joints. *Eng. Fail. Anal.* 13 (2006) 1410–1421.

[5] T.N. Chakherlou, R.H. Oskouei, J. Vogwell, Experimental and numerical investigation of the effect of clamping force on the fatigue behaviour of bolted plates. *Eng. Fail. Anal.* 15 (2008) 563–574.

[6] T.N. Chakherlou, J. Vogwell, The effect of cold expansion on improving the fatigue life of fastener holes. *Eng. Fail. Anal.* 10 (2003) 13–24.

[7] R.G. Budynas, J.K. Nisbett, Shigley's Mechanical Engineering Design, eighth ed., McGraw-Hill Series in Mechanical Engineering, London, 2008.

[8] A. Skorupa, M. Skorupa, T. Machniewicz, A. Korbel, Fatigue crack location and fatigue life for riveted lap joints in aircraft joints in aircraft fuselage. *Int. J. Fatigue.* 58 (2014) 209-17.

[9] J. Mucha, The effect of material properties and joining process parameters on behaviour of self-pierce riveting joints made with the solid rivet. *Mater. Des.* 52 (2013) 932-946.

[10] T.N. Chakherlou, Y. Alvandi-Tabrizi, A. Kiani, On the fatigue behaviour of cold expanded fastener holes subjected to bolt tightening, *Int. J. Fatigue* 33 (2011) 800–810.

[11] T.N. Chakherlou, M. Mirzajanzadeh, B. Abazadeh, K. Saeedi, An investigation about interference fit effect on improving fatigue life of a holed single plate in joints. *Eur. J. Mech. A Solid* 29 (2010) 675–682.

[12] T.N. Chakherlou, M. Mirzajanzadeh, J. Vogwell, Experimental and numerical investigations into the effect of an interference fit on the fatigue life of double shear lap joints. *Eng. Fail. Anal.* 16 (2009) 2066–2080.

[13] D. Croccolo, M. De Agostinis, L. Ceschini, A. Morri, A. Marconi, Interference fit effect on improving fatigue life of a holed single plate. *Ffems* 36 (2013) 689–698.

[14] K. Iyer, S.J. Hu, F.L. Brittman, P.C. Wang, D.B. Hayden, S.P. Marin, Fatigue of single- and double-rivet self-piercing riveted lap joints. *Fatigue Fract. Eng. Mater. Struct.* 28 (2005) 997–1007.

[15] E. Armentani, R. Citarella, DBEM and FEM analysis on non-linear multiple crack propagation in an aeronautic doubler-skin assembly. *Int. J. Fatigue* 28 (2006) 598–608.

[16] R.H. Oskouei, M. Keikhosravy, C. Soutis, A finite element stress analysis of aircraft bolted joints loaded in tension. *The Aeronautical Journal.* 114 (2010) 315–320.

[17] J. Kim, J.C. Yoon, B.S. Kang, Finite element analysis and modelling of structure with bolted joints. *Appl. Math. Model* 31 (2007) 895–911.

[18] S. Sathiya Narayan, D.V.T.G. Pavan Kumar, Satish Chandra, Implication of unequal rivet load distribution in the failures and damage tolerant design of metal and composite civil aircraft riveted lap joints. *Eng. Fail. Anal.* 16 (2009) 2255-2273.

[19] D.V.T.G. Pavan Kumar, S. Sathiya Narayan, S. Kalyana Sundaram, Satish Chandra, Further numerical and experimental failure studies on single and multi-row riveted lap joints. *Eng. Fail. Anal.* 20 (2012) 9-24.

[20] N. Chen, H. Luo, M. Wan, J. Chenot, Experimental and numerical studies on failure modes of riveted joints under tensile load. *J. Mater. Process. Technol.* 214 (2014) 2049–2058.

[21] L.J. Hart-Smith, Bolted joint analyses for composite structures—Current empirical methods and future scientific prospects, ASTM Special Technical Publication (2004) 127-160.

[22] S.D. Thoppul, J. Finegan, R.F Gibson, Mechanics of mechanically fastened joints in polymer–matrix composite structures—A review. *Compos. Sci.Technol.* 69 (2009) 301–329.

[23] A. Atas, N. Arslan, F. Sen, Failure analysis of laminated composite plates with two parallel pin-loaded holes. *J. Reinf. Plas.* 28 (2009) 1265–1276.

[24] A. Baker, S. Dutton, D. Kelly, Composite Material for Aircraft Structures, second ed., American Institute of Aeronautics and Astronautics: Reston, USA, 2004.

[25] A.A. Pisano, P. Fuschi, D.D. Domenico, Failure modes prediction of multi-pin joints FRP laminates by limit analysis. *Compos. Part. B* 46 (2013) 197–206.

[26] M. Keikhosravy, R.H. Oskouei, P. Soltani, A. Atas, C. Soutis, Effect of geometric parameters on the stress distribution in Al 2024-T3 single-lap bolted joints. *Int. J. Struct. Integr.* 3 (2012) 79–93.

[27] Nabil Chowdhury, Wing Kong Chiu, John Wang, Paul Chang, Static and fatigue testing thin riveted, bonded and hybrid carbon fiber double-lap joints used in aircraft structures. *Compos. Struct.* 215 (2015) 315-323.

[28] A.A. Baker, R. Jones (Eds.), *Bonded Repair of Aircraft Structures*, Martinus Nijhoff Publishers, Dordrecht, 1988, pp. 49-106

[29] R. Jones, Bonded repair of damage. *J. Aero. Soc. (India)* 36 (1984) 193-201.

[30] L.R.F. Rose, An application of the inclusion analogy for bonded reinforcements. *Int. J. Solids Structures* 17 (1981) 827-838.

[31] M.M. Ratwani, A parametric study of fatigue crack growth behavior in adhesively bonded metallic structures. *J. Eng. Mats. And Tech.* 100 (1978) 46-51.

[32] C.T. Sun, J. Klug, C. Arendt, Analysis of cracked aluminium plates repaired with bonded composite patches. *AIAA Journal* 34 (1996) 369-374.

[33] M.J. Young, D.P. Rooke, D.J. Cartwright, Analysis of patched and stiffened cracked panels using the boundary element method. *Int. J. Sol. Struct.* 29 (1992) 2201-2216.

[34] M.D. Banea, L.F.M. da Silva, Adhesively bonded joints in composite materials: an overview. *Proc. IMechE, Part L: J. Mater. : Design and appl.* 223 (2009) 1-18.

[35] R.J Clark, D.P. Romilly, Bending of bonded composite repairs for aluminium aircraft structures: a design study. *J. Aircraft*. 44 (2007) 2012-2025.

[36] S. Gòmez, J. Oñoro, J. Pecharromán, A simple mechanical model of a structural hybrid adhesive/riveted single-lap joint. *Int. J. Adhes. Adhes.* 27 (2007) 263-267.

[37] A. Pirondi, F. Moroni, Clinch-bonded and rivet-bonded hybrid joints: application of damage models for simulation of forming and failure. *J. Adhes. Sci. Technol.* 23 (2009) 1547-1574.

[38] T. Sadowski, M. Knec, P. Golewski, Experiment investigations and numerical modelling of steel adhesive joints reinforced by rivets. *Int. J. Adhes.Adhes.* 30 (2010) 338-346.

[39] G. Kelly, Quasi-static strength and fatigue life of hybrid (bonded/bolted) composite single-lap joints. *Compos. Struct.* B 72 (2006) 119-129.

[40] J. Hart-Smith, Bolted and bonded joints, *ASM handbook,* 21 (1998)167-176.

[41] J.H. Kweon, J.W. Jung, T.H. Kim, J.H. Choi, D.H. Kim, Failure of carbon composite-to-aluminium joints with combined mechanical fastening and adhesive bonding. *Compos. Struct.* 75 (2006) 192-198.

[42] C.T. Sun, K. Bhawesh, P. Wang, R. Sterkenburg, Development of improved hybrid joints for composite structures. *Compos. Struct.* 35 (2005) 1-10.

[43] Hart-Smith, L.J. Bonded-bolted composite joints. *J. Aircraft* 22 (1985) 993-1000.

[44] A. Barut, E. Madenci, Analysis of bolted-bonded composite single-lap joints under combined in-plane and transverse loading. *Compos. Struct.* 88 (2009) 579-594.

[45] G. Kelly, Load transfer in hybrid (bonded/bolted) composite single-lap joints. *Compos. Struct.* 69 (2005) 35-43.

[46] E. Paroissien, M. Sartor, J. Huet, F. Lachaud, Analytical two-dimensional model of a hybrid single-lap-joint. *J. Aircraft* 44 (2007) 573-82.

[47] R. Matsuzaki, M. Shitaba, A. Todoroki, Improving performance of GFRP-aluminium single-lap joints using bolted-co-cured hybrid method. *Comps. A: Appl. Sci. Manuf.* 39 (2008) 154-163.

[48] United States Department of Transportation (2012). Aviation Maintenance Technician Handbook-Airframe. Chapter 4 pp. 31-57.

[49] Aerospace Engineering, http://www.aerospacengineering.net/?p=244 (accessed 8.17.17)